[American Journal of Science, Vol. 307, May, 2007, P. 833–855, DOI 10.2475/05.2007.03]

MINERAL SOLUBILITY AND HYDROUS MELTING RELATIONS IN THE DEEP EARTH: ANALYSIS OF SOME BINARY *A*–H_2O SYSTEM PRESSURE-TEMPERATURE-COMPOSITION TOPOLOGIES

ALISTAIR C. HACK*,**†, JÖRG HERMANN**, and JOHN A. MAVROGENES**,§

ABSTRACT. Phase relations involving hydrous melting, volatile and mineral solubility and supercritical fluid phenomena at high pressure for mineral–H_2O systems are generally not completely constrained by experimental data or adequately treated in thermodynamic models. Here we examine geometric relations in pressure (*P*)-temperature (*T*)-composition (*X*) topologies of simple hydrous *A*–H_2O binaries, thus avoiding some of the pitfalls associated with other approaches. The relations between mineral solubility surfaces, wet melting and critical L=V behavior are shown explicitly in a series of *PT*, *TX* and isopleth contoured *PT* projections. Our analysis highlights the significance of Clapeyron slopes of melt- and fluid-solubility isopleths for L+V coexistence, supercritical-fluid phenomena and the geometry of phase-equilibrium boundaries. The results are useful for understanding wet melting, magma degassing and fluid behavior in high-pressure metamorphic and subduction-zone environments. The diagrams illustrate the general pattern of mineral solubility in aqueous fluids and volatile solubility in silicate melts. We discuss the significance of the critical-curve geometry for phase relations and fluid/melt densities. We examine a continuum of phase relation topologies for *A*–H_2O, and show that these can result from subtle but important differences in the compositional behavior of melt coexisting with H_2O-rich fluid. The systems SiO_2(quartz)–H_2O and $NaAlSi_3O_8$(albite)–H_2O are taken as examples for which there is experimental data available to calibrate a complete phase relation topology.

INTRODUCTION

Recently there has been renewed interest in the nature and occurrence of supercritical fluids with hydrous-melt-like properties in geological processes. This renaissance is due mostly to the recognition that pressure, temperature conditions in subduction zones might be suitable to form supercritical fluids (for example, Massonne, 1992; Sharp and others, 1993; Scambelluri and Philippot, 2001; Hermann, 2003; Audétat and Keppler, 2004; Kessel and others, 2005a, 2005b; Hermann and others, 2006).

Considerable uncertainty attends discussion of the role and nature of fluids in deep-seated geological processes. In part this is because natural fluids are ephemeral, so that the details of fluid–rock interactions must be inferred indirectly, for example from major and trace element depletions or enrichments (Ague, 1994a, 1994b, 1997). Although fluid inclusions are occasionally identified in high-temperature, high-pressure rocks, their provenance is usually equivocal and/or they have decrepitated during exhumation (Invernizzi and others, 1998; Scambelluri and others, 2001; Ferrando and others, 2005).

Experimental studies and thermodynamic models of phase equilibria and solubility relations in rock–H_2O systems provide independent constraints on the behavior and composition of minerals, fluids and melts at high-pressure and -temperature conditions. However, large regions of pressure-temperature-composition (*PTX*) space

*Institute for Mineralogy and Petrology, ETH Zürich, Zürich 8092, Switzerland
**Research School of Earth Sciences, The Australian National University, Canberra, ACT 0200, Australia
§Department of Earth and Marine Sciences, The Australian National University, Canberra, ACT 0200, Australia
†Corresponding author: alistair.hack@erdw.ethz.ch

remain experimentally unexplored even for simple systems like SiO_2–H_2O and $NaAlSi_3O_8$(albite)–H_2O, with fluid compositions being probably the least known. Similarly, thermodynamic models (for example, Holland and Powell, 1998, 2001) typically do not treat all experimentally observed phenomena, such as complete fluid–melt miscibility (for example, Kennedy and others, 1962; Shen and Keppler, 1997; Kessel and others, 2005a, 2005b), reflecting the paucity of data to calibrate thermochemical models.

Theoretical descriptions of the general *PTX* phase relation topology for various types of simple two component (*A*–H_2O) systems have been available for a long time (for example, Morey and Niggli, 1913). However, these are seldom used except schematically in the geological literature. This is because, until recently, experimental constraints for real systems were insufficient to construct calibrated topologies. These kinds of topological frameworks can be integrated with fragmentary experimental data to circumvent limitations imposed by incomplete thermodynamic models and experimental data, to provide both conceptual insights and predictive constraints on the compositional behavior of each phase (for example, fluid and melt) over the entire *PT* space.

In this paper we examine a topological framework for a generic two-component silicate–water system (*A*–H_2O), with a minimum of schematic distortion and explicitly show the systematics of how fluid and melt compositions relate to the phase relations, for example, the wet solidus and critical phenomena. Using this framework, we construct a semi-quantitative model of the system SiO_2–H_2O, which predicts the composition of the buffered fluid at any *P* and *T*. We discuss the general implications of the results, highlight the constraints imposed by experimental data and the phase relations that remain possible, yet rarely considered. The aim of this contribution is to clarify the links between changes in *PT*, fluid and melt compositions, and phase relations for simple systems.

BACKGROUND

The topological configuration of simple two-component systems (*A*–H_2O) in which one component is highly volatile (H_2O) has been known since at least Morey and Niggli (1913). Numerous detailed discussions of these ideal relations are available (for example, Ricci, 1951; Morey, 1957; Wyllie and Tuttle, 1960; Fyfe and others, 1978; Paillat and others, 1992; Manning, 2004; Veksler, 2004). Accordingly, only a brief summary is given here. In this paper we broadly follow the nomenclature given in Boettcher and Wyllie (1969a). A brief glossary of the terms and abbreviations is given in table 1.

One-component systems, like H_2O or *A*, have a liquid+vapor coexistence curve that at high-temperature terminates at a critical point (fig. 1, for H_2O: T_{crit} = 374 °C, P_{crit} = 22.1 MPa, critical density = 0.32 g/cm^3, Haar and others, 1984). With increasing temperature along this curve, the properties of the liquid and vapor converge to the extent that liquid and vapor become indistinguishable at the critical point (analogous to the closing of a miscibility gap or solvus). At *T* and *P* above the critical point, a single supercritical fluid is stable. In the two-component system *A*–H_2O, a L=V critical curve connects the critical points in the end-member systems. Along the L=V critical curve liquid and vapor are indistinguishable, the curve represents the maximum *P, T* and *X* extent of the liquid–vapor miscibility gap (that is, the *PT* loci of the L–V solvus crest). At *T, P* above the critical curve one, supercritical, fluid is stable. Though not obvious from figure 1, the critical composition along the critical curve varies continuously from H_2O to *A* between the respective critical points. A second curve defined by the coexistence of three phases, solid-*A*+liquid+vapor, extends from the low-temperature *A*–H_2O eutectic point to the triple point for *A* (solid+liquid+vapor) where it terminates, is termed the solubility curve (fig. 1).

TABLE 1
Symbols used

P	Pressure 1 bar = 10^5 Pa, 1 GPa = 10^4 bar = 10 kbar
T	Temperature usually as celsius, otherwise kelvin
X	Composition (usually by weight, otherwise molar)
A	silicate, the non-volatile component, in the solid state at room conditions
S_A	pure *A* in the solid state*
L_A	pure *A* in the liquid state
G_A	pure *A* in the vapor state
H_2O	water, in the liquid state at ambient *T,P*, the volatile component
ice	pure H_2O in the solid state
steam	pure H_2O in the vapor state
A–H_2O	simple binary system of interest
V	aqueous Vapor (=H_2O with dissolved A)
L	hydrous Liquid/melt (=L_A with dissolved H_2O)
Eut(H_2O–S_A)	H_2O–S_A eutectic point, where ice+S_A+L+V are in equilibrium
Trip.pt H_2O	triple point of pure H_2O (L+V+S)
Trip.pt *A*	triple point of pure *A* (L+V+S)
kH_2O	L=V critical point on the boiling curve of H_2O
*k*A	L=V critical point on boiling curve of pure *A*
k_1(L=V)A	lower L=V critical endpoint on the vapor+liquid coexistence curve where A is stable as a solid in the binary *A*–H_2O
k_2(L=V)A	upper L=V critical endpoint in the binary *A*–H_2O wet solidus (A is stable as a solid at this point)
L=V	the condition where L and V become indistinguishable at the closure of the L+V solvus
SCF	SuperCritical Fluid, a completely miscible continuous solution. Where SCF is stable L and V do not coexist as immiscible phases

**A* is refractory (or has low-volatility) as it is solid (S_A) under most of the *PT* conditions considered (unless specified)

Morey and Niggli (1913) recognized two basic types of *A*–H_2O topology based on whether the critical and solubility curves remain separated (fig. 1A) or intersect in *PTX* (fig. 1B). The first type of behavior is characteristic of systems in which solid *A* is highly soluble in H_2O, a geological example is NaCl–H_2O (Sourirajan and Kennedy, 1962). The second type, where the critical and solubility curves intersect, is characteristic of systems in which solid *A* is sparingly soluble in H_2O (for example, SiO_2–H_2O, Kennedy and others, 1962). In this study we are concerned only with the second type, as it is appropriate generally to silicate–H_2O systems.

Intersection of the solubility and critical curves produces two separate *P, T* regions where a liquid–vapor miscibility gap is stable and there is a discontinuity in the solubility curve (fig. 1B). In the geological literature, the high-temperature and low-temperature segments of the solubility curve are commonly called the wet solidus and the vapor-saturation curve, respectively. The ability to predict regions of immiscibility is of obvious geochemical interest, as immiscible phases have different chemistries and physical properties (viscosity and density). Hence L+V immiscibility can lead to a spatial fractionation of the dissolved mass (for example, Hedenquist and Lowenstern, 1994; Heinrich and others, 1999; Sun and others, 2003).

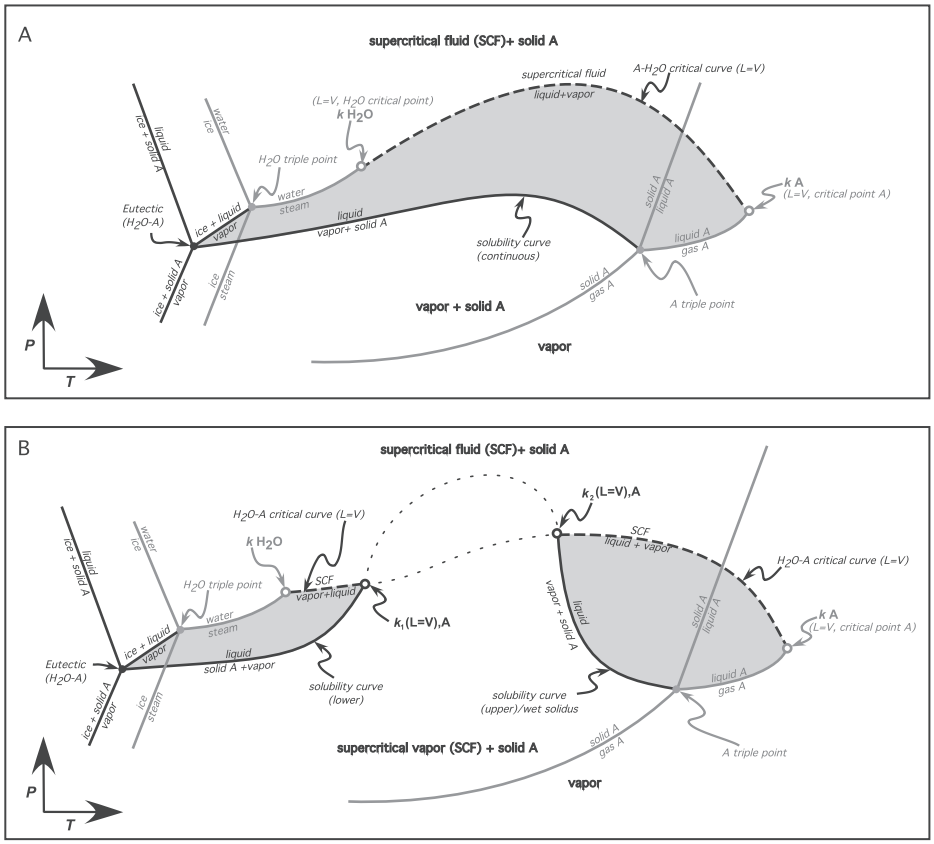

Fig. 1. Schematic *PT* projections illustrating two contrasting binary eutectic *A*–H_2O topologies where, (A) solubility curve (S+V=L; solid) and critical curve (L=V; dashed) do not intersect, an example is NaCl–H_2O; and, (B) solubility curve (solid) and critical curve (dashed) intersect, examples include SiO_2–H_2O and $NaAlSi_3O_8$–H_2O. Gray fields indicate where a liquid+vapor miscibility gap is stable. Gray curves = end-member equilibria; black curves = binary system equilibria. Curves (dotted) between critical endpoints k_1(L=V)A and k_2(L=V)A are imaginary/metastable (after Morey and Niggli, 1913).

Two-dimensional, isobaric *TX* sections reveal the manner in which phase stability and composition are related to the phase-equilibrium boundaries projected in *PT* (fig. 2).

VAPOR, MELT AND SUPERCRITICAL FLUID COMPOSITIONS ON *PT* PROJECTIONS

General Construction and Discussion of Some Important Aspects

To overcome the shortcomings of schematic diagrams, we present for the first time *PT* projections in which liquid, vapor and supercritical fluid compositions are completely shown. Changes in fluid and liquid compositions on a *PT* projection can be expressed explicitly by using various continuous, composition iso-lines (isopleths) for each phase. Here we use this method to clarify the relations indicated on figures 1 and 2. We focus our discussion on the high-temperature melting relations involving melt and vapor and supercriticality.

Examination of figure 2 shows that there are four distinct saturation-surfaces involving liquid and vapor in the binary *A*–H_2O that need to be represented: 1) the subsolidus fluid (V) composition at saturation with mineral-*A*; 2) the supersolidus

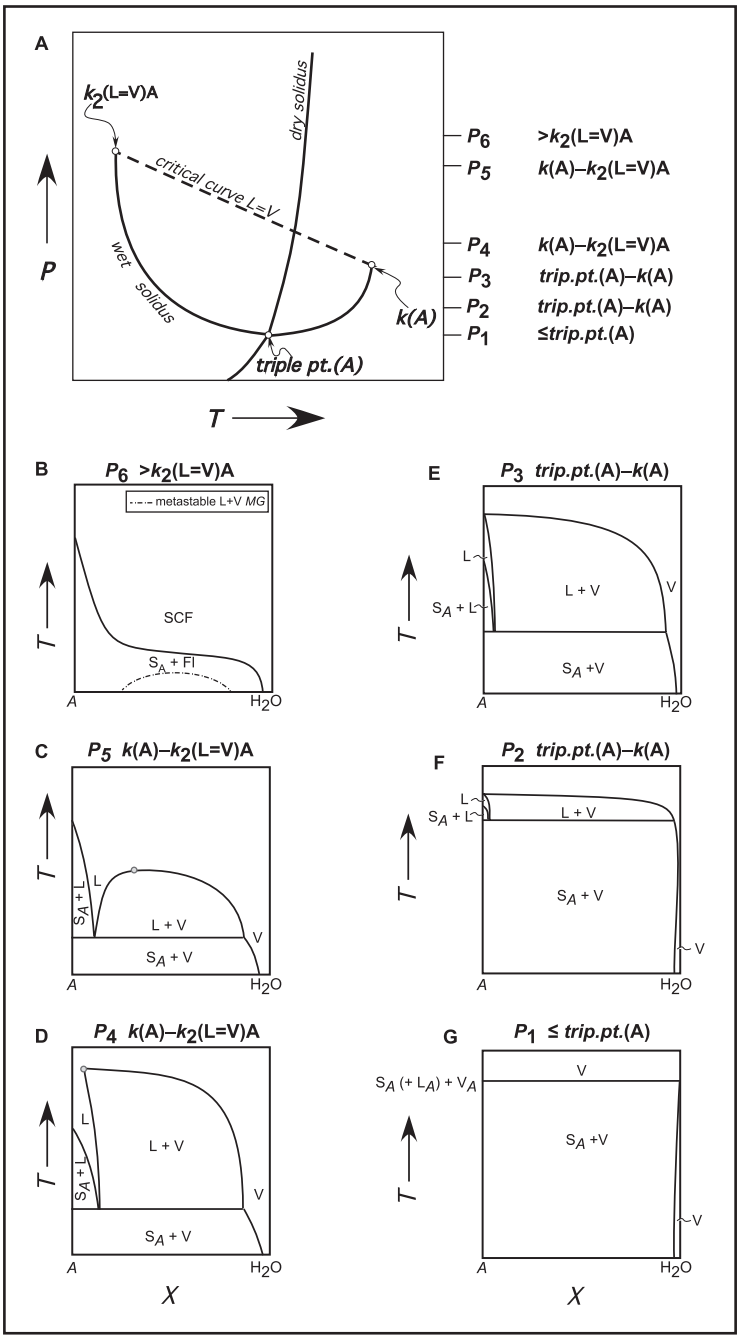

Fig. 2. Schematic showing relations between *PT* projection (A) and isobaric *TX* sections (B–G) for an *A*–H_2O system where the solubility curve and critical curve intersect, analogous to a silicate–H_2O system ('type-2', fig. 1B). The L+V miscibility gap ('*MG*', dashed curve, B) is shown as metastable below the solubility curve at pressures higher than the critical endpoint of the wet solidus, implying that the metastable projection of the critical curve also has a negative d*P*/d*T* slope.

liquid (melt) composition at saturation with mineral-*A*; 3) the supersolidus vapor composition in equilibrium with the coexisting melt; and 4) the supersolidus liquid composition at saturation with vapor. Some of these surfaces (represented by isopleths) are continuous, but inflected, across phase-equilibrium boundaries. For example, at *P* below the wet solidus endpoint, vapor is stable on both the high- and low-temperature sides of the wet solidus. While vapor isopleths are inflected at the wet solidus they are continuous to higher temperature. At the wet solidus, the other phase with which vapor coexists changes from crystalline-*A* at lower *T* to hydrous liquid (L) at higher temperature (fig. 2C). A two-phase L+V field terminates along a critical curve (fig. 2B). At the critical curve coexisting L and V isopleths of the same composition intersect, hence L=V. L and V are immiscible at *P* and *T* below the critical endpoint on the wet solidus, here denoted as k_2(L=V)A. Mineral-*A* is a stable phase at the critical endpoint on the wet solidus. At higher *P* and *T* than the critical endpoint, the wet solidus has vanished and crystalline-*A*-saturated vapor and liquid fields are continuous.

Figure 3 schematically illustrates the manner in which liquid and vapor compositional isopleths relate to various phase equilibrium boundaries, especially at the wet solidus, L=V critical curve and their terminations. Other notable points include: 1) the isopleth location within the liquid+vapor field above the wet solidus is arbitrary. That is the compositions derived from the figure at a fixed *P* and *T* are not quantitatively constrained, they are schematic; 2) the relative isopleth positions and slope are constrained because the isopleth geometry determines the shape of the solvus in this field. The isopleth geometry corresponds to the general behavior shown in figure 2; and, 3) the broad framework of mineral-*A* solubility isopleths in the supercritical field is based on data for SiO_2–H_2O (for example, Manning, 1994). The solubility relations near the lower critical endpoint (k_1) and the implications of various modifications of figure 3 are considered in more detail below.

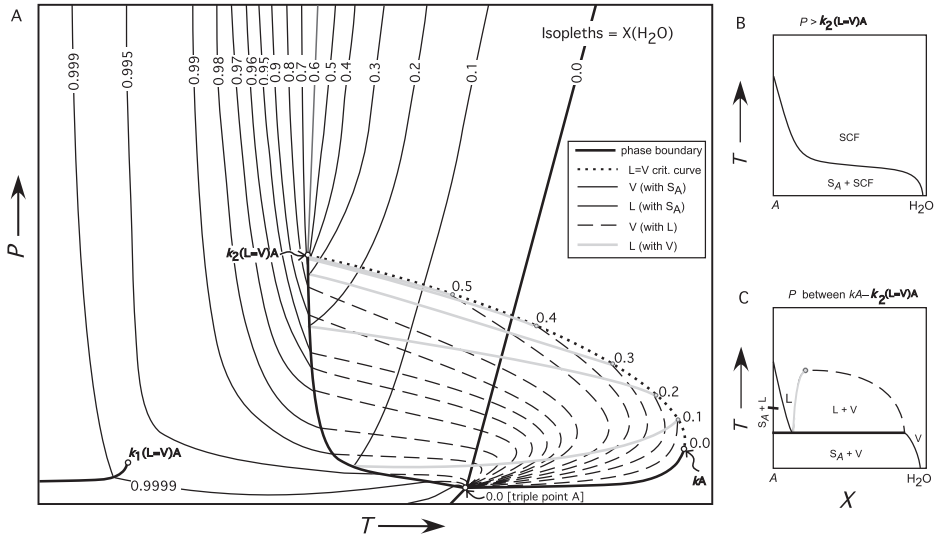

Fig. 3. (A) Composition projected as isopleths (thin curves) onto the *PT* surface for a 'type-2' system, mineral *A*–H_2O, in which the critical curve intersects the solubility curve (figs. 1B and 2). Equilibrium phase boundaries (bold curves), V-saturated L composition (thin dashed) intersects the coexisting V composition (thin unbroken curves) at the L=V critical curve (bold dashed line). A single upper critical isopleth, here $X(H_2O)$ = 0.6, extends from k_2(L=V)A, a different lower critical isopleth extends from k_1(L=V)A occurring between 0.999–0.9999 $X(H_2O)$ (not shown). (B) and (C) are isobaric *TX* sections through the *PT* phase relations.

Figure 3 shows that the wet solidus terminates into a divariant field at the intersection with a critical (L=V) curve, at which vapor and liquid converge in composition. At the critical endpoint on the wet solidus, mineral-*A* coexists with a supercritical fluid of fixed composition. In the divariant field, mineral-*A* may coexist with a supercritical-fluid, the fluid composition depends on both *T* and *P*. The critical composition at the wet solidus endpoint extends as a line in *PT*. The composition of supercritical fluid coexisting with mineral-*A* may vary continuously, but will be more liquid-like or vapor-like depending on the *P* and *T*, relative to the *PT* location of the critical composition. At *T* above the triple point of *A*, the liquid+vapor curve for *A* is also the zero-H_2O isopleth for liquid+vapor and it terminates at *k*A. All other *A*–H_2O liquid and vapor isopleths of the same composition are separated in the liquid+vapor field, except where they intersect at the critical curve. The range of fluid compositions occurring along the L=V critical curve fall between the critical composition at k_2(L=V)A and pure *A* at *k*A (and *trip.pt.*A, fig. 3).

Ideal simple binary system topologies have certain limitations. An example is the requirement that all hydrous vapor originate at the triple point for a single anhydrous end-member (*A*), whereas more complex systems will contain more than one end-member anhydrous triple point. For more complex solutions, it is not usually obvious which parts of the equilibria in a *PT* projection will be seen by a particular bulk composition, given that the compositions of the phases, here L and V, vary along the univariant lines.

Paillat and others (1992) presented a three-dimensional *PTX* model of solid–liquid–vapor phase relations for $NaAlSi_3O_8$(albite)–H_2O. The topology they describe is analogous to the *A*–H_2O system shown in figure 3 but does not extend up to *P* of the wet solidus critical endpoint, k_2(L=V)Alb (their diagram may be of assistance in visualizing our contoured version). In the following section, we discuss the significance of the d*P*/d*T* geometry of liquid and vapor compositional isopleths, critical curves and relative *P,T* positions of points k_2(L=V)A, *k*A, and *trip.pt.*A.

Critical Points and L=V Curve Geometries, Isopleth Slopes and Their Relation to Mineral Solubility and the Fluid–Melt Solvus

Here we focus on L+V immiscibility and the geometry of the critical curve (fig. 4). The d*P*/d*T* slopes of fluid and melt isopleths directly reflect the *PTX* behavior of the L+V solvus. For clarity, these lines are not shown on figure 4. The key aspect of figure 4 is the illustration of how critical curve geometries relate to immiscibility and govern solubility behavior. Different topological configurations arise from contrasting d*P*/d*T* and d*T*/d*X* (or d*P*/d*X*) behavior of hydrous liquid and aqueous vapor compositions. Curvature and fanning of coexisting immiscible L and V isopleths in *PT* relates directly to the solvus geometry. Isopleths have additional chemical meaning, as they indicate the *P* and *T* dependence of solubility (in L or V), which reflects the underlying dissolution mechanisms.

From a geometric perspective, it is principally the *PT* location of the invariant and critical points in *A*–H_2O that determines the average d*P*/d*T* slope of the equilibrium phase boundaries, and hence also that of the various isopleths. In figure 4A, the critical endpoint on the solidus k_2(L=V)A occurs at a lower pressure than *k*A. As a result, the critical curve requires an overall positive d*P*/d*T*. The L+V miscibility gap in this system is encountered at pressures above the end of the wet solidus for appropriate compositions, but not in the presence of a mineral.

Figure 4B shows a critical (L=V) curve that develops a *P* maximum above the critical endpoint of the wet solidus. The accompanying isobaric *TX* section shows how the L+V solvus is isolated at higher *T* than the solubility surface, rather than at lower *T*. The isobar intersects the critical curve at two temperatures, producing an island of L+V immiscibility above the second critical endpoint in the absence of a wet solidus.

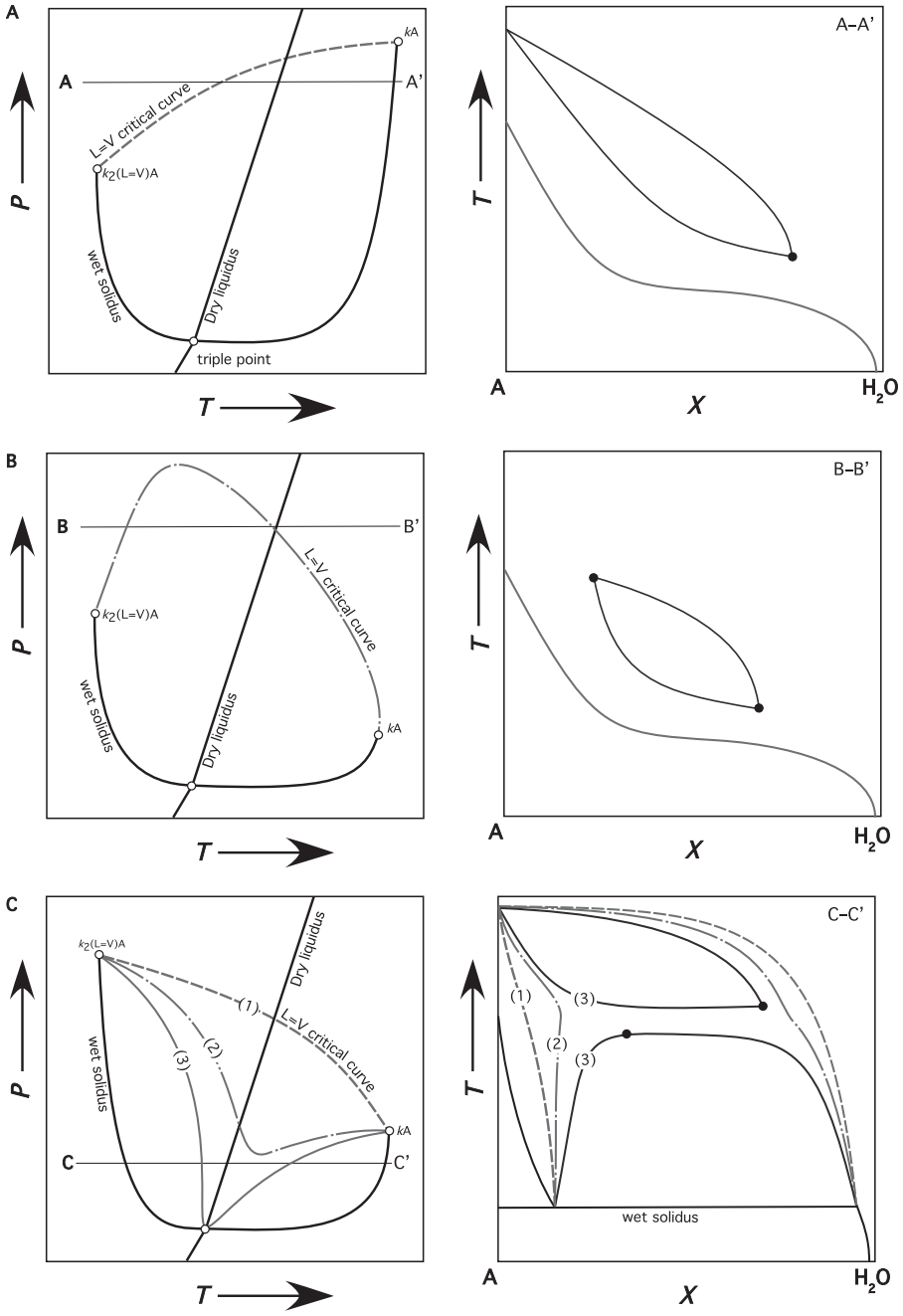

Fig. 4. Illustration of relations between critical curve geometry and fluid–melt solvus behavior. (A) Positive dP/dT critical curve where $P\,k_2$(L=V)A < $P\,k$A. (B) Critical curve with P maximum above k_2(L=V)A and kA. (C) Where critical points $P\,k_2$(L=V)A > $P\,k$A and comparing critical curves: (1) having entirely negative dP/dT; (2) with P minimum between k_2(L=V)A and kA; and (3) intersecting with the triple point for pure A from higher and lower T. Open circles represent critical endpoints; filled circles indicate where the TX sections cut the critical curve.

Figure 4C, shows three different critical L=V curve arrangements and accompanying isobaric *TX* sections (c–c') showing the L+V solvi which produce these curves. An important observation is that reversals isopleth d*P*/d*T* correspond to a d*T*/d*X* slope reversal in the L+V solvus limb(s). These inflections suggest that the L+V miscibility gap is characterized by two solvi components. Isopleth slope reversals, where no phase transitions are involved in the coexisting minerals, could be associated with chemical coordination changes in either the V or L phases. The case where the 'low' and 'high' L+V solvi are completely separated is shown by curve '3' (fig. 4C). Here, solubility isopleths do not reverse d*P*/d*T,* but maintain positive *or* negative slope within each L+V field. Relations associated with critical L+V curve '3' are discussed further below.

Clapeyron Slope of Critical L= V Curves

Unfortunately, the physical properties of silicate-bearing aqueous fluids are poorly known (for example, density). Nonetheless, the fundamental systematics for volumetric properties of supercritical and immiscible fluid mixtures are known from simple thermodynamic relations (for example, Rowlinson, 1983; Levelt Sengers, 2000). The latter allow us to make some simple statements regarding the relative physical properties of miscible and immiscible fluids.

The geometry of critical phase boundaries contains information about the physical properties of the phases involved. For example, at constant temperature, if a mixture of L+V becomes completely miscible with increasing pressure, it is because the homogeneous phase has a higher density than the coexisting immiscible L+V. The slope of an equilibrium boundary, such as the L=V critical curve, is defined by the Clapeyron relation: $dP/dT = \Delta S / \Delta V$. If the boundary is a straight line, then the values of ΔS (entropy of reaction) and ΔV (volume of reaction) are not dependent upon T and P. A negative d*P*/d*T* slope implies that ΔS and ΔV have opposite signs, while for positive d*P*/d*T,* ΔS and ΔV have the same sign. Thus, the slope (and curvature) of critical curves has a simple thermodynamic significance and provides information on the nature of the relative compressibilities of L+V and supercritical fluids.

So far, L=V critical curves reported in hydrous silicate systems ($NaAlSi_3O_8$–H_2O, Shen and Keppler, 1997; $NaAlSiO_4$–H_2O, $NaAlSi_2O_6$–H_2O, 'haplogranite'–H_2O, Bureau and Keppler, 1999; $NaAlSi_3O_8$–$H_2O \pm Na_2O \pm B_2O_3 \pm F_2O_{-1}$, Sowerby and Keppler, 2002) show negative d*P*/d*T* slopes and are nearly linear, within the experimental uncertainty. In these cases the supercritical region lies on the high-pressure side of the critical curve. Accordingly, we expect high-pressure critical fluids to be more compressible than equivalent immiscible L+V mixtures. A negative d*P*/d*T* also implies that cooling of a supercritical solution results in L+V unmixing. However, note that there is evidence that some silicate–H_2O critical curves possess positive d*P*/d*T*; for example, parts of the system Na_2SiO_3–SiO_2–H_2O (Urusova and Valyashko, 2001). Critical (L=V) curves with positive d*P*/d*T* allow immiscible L+V mixtures to evolve into supercritical solutions on cooling.

Additionally, it is possible that some L=V critical lines may be curved to the extent that *T* minima (or maxima) occur. The theoretical analysis by Boettcher and Wyllie (1969a) of wet melting relations and critical curves in a ternary MO–SiO_2–H_2O system suggests that the occurrence of *P,T* minima (and maxima) on critical curves is practically unavoidable in non-binary, higher-order systems. Significantly, a *T* minimum (or maximum) on a critical curve implies $\Delta V = 0$ and requires a density inversion amongst the phases at the critical curve. A density inversion need not accompany a significant change in the coexisting fluid compositions. Thus, with increasing pressure the hydrous silicate liquid would become relatively less dense and eventually more buoyant than the H_2O-rich fluid at high *P*. An example of L–V density inversion occurs in the binary CO_2–H_2O system close to 0.23 GPa (Tödheide and Franck, 1963; Takenouchi and Kennedy, 1964).

GEOMETRICALLY CONSISTENT *PTX* RELATIONS FOR AN INCOMPLETELY DETERMINED SYSTEM: SiO_2–H_2O AS AN EXAMPLE

Mineral solubility and wet melting relations in the SiO_2–H_2O system have been the subject of numerous investigations (table 2). Figure 5 shows a representative compilation of experimental knowledge of SiO_2–H_2O. Respectively, the two critical endpoints, k_1(L=V)Qtz and k_2(L=V)Qtz, are located near $k H_2O$ (374 °C, 22.1 MPa; Haar, and others, 1984) and at 1100 °C, 0.97 GPa, ~0.47 $X(SiO_2)$ (Kennedy and others, 1962). Guissani and Guillot (1996) calculated that the critical point for pure silica, $kSiO_2$, occurs at 11,700 °C, ~0.2 GPa and critical density = 0.58 g cm^{-3}. In the binary system SiO_2–H_2O, the upper *PT* region in which L+V immiscibility occurs is less well constrained. The location of the critical curve (L=V) (dashed curve, fig. 5B) is not presently known – except in the vicinity of the quartz wet solidus (Qtz+V=L) where it terminates by intersection with the L=V critical curve (Kennedy, and others, 1962). At higher temperature, the binary critical (L=V) curve intersects the critical point (L_{SiO2}=V_{SiO2}) of pure silica $kSiO_2$ (fig. 3). The location of critical endpoints k_2(L=V)Qtz and $kSiO_2$ indicates that the L=V critical curve has an average negative d*P*/d*T* slope (approximately, -0.073 MPa K^{-1}, for linear d*P*/d*T*). The available data for SiO_2–H_2O can thus be described by a type-2 topology as described above (see fig. 1B and fig. 3).

Figure 5B schematically shows the phase relations for SiO_2–H_2O near the upper three-phase (Qtz+V=L) curve, along with *PT* stability of the different SiO_2 polymorphs. Figure 5C shows the composition of V-saturated liquid at different temperatures for a series of pressures, expressed as mole fraction water $X(H_2O)$. Below 0.4 GPa there is little or no temperature dependence of H_2O solubility in the liquid. Above 0.5 GPa, as k_2(L=V)Qtz is approached, H_2O solubility strongly increases with increasing temperature. L and V compositions converge to one critical composition (or supercritical fluid, SCF) at the upper or second critical endpoint on the wet solidus. Figure 5E shows an isobaric *TX* section through figure 5A at 0.4 GPa. Figures 5D and 5F show measured SiO_2 solubility in H_2O at 1.5 GPa as a function of temperature, expressed in weight percent (H_2O) and mole fraction $X(H_2O)$, respectively. The L+V miscibility gap is gone at this pressure, $P > k_2$(L=V)Qtz (solvus is shown metastable at a lower temperature than the solubility curve). There is a continuous transition from dry SiO_2 liquid (L_{SiO2}) to almost pure H_2O liquid, without passing through a wet melting reaction. L and V are completely miscible and a single fluid phase stably coexists with solid-SiO_2 at these conditions; the fluid is supercritical.

Observations by Nakamura (1974) that show quartz solubility is continuous with increasing temperature (up to the melting point) appear to leave little doubt that in SiO_2–H_2O the quartz wet solidus is no longer defined at 1.5 GPa. Moreover, it is worth recognizing that the different quartz solubility data sets are in good general agreement and support the melting relations and critical endpoint on the wet solidus observed by Kennedy and others (1962). Similar agreement is observed between Anderson and Burnham (1965), Kennedy and others (1962) and Holtz and others (2000) at pressures where the wet solidus is still present (figs. 5C and 5E), and also on the *T* dependence of quartz solubility in H_2O at 1.5 GPa (above the end of the wet solidus) determined by Nakamura (1974) and Manning (1994; figs. 5D and 5F).

Insights from Water Solubility and Supercriticality in the System $NaAlSi_3O_8$(albite)–H_2O

Like SiO_2–H_2O, $NaAlSi_3O_8$–H_2O appears to be a type-2 system topology albeit with additional complexities, for example with increasing pressure albite breaks down to jadeite + quartz (Holland, 1980; Liu and Bohlen, 1995).

Figure 6A indicates experimentally investigated *P,T* conditions in the albite–water ($NaAlSi_3O_8$–H_2O) system (a representative selection from table 2). Figure 6B shows a schematic *PT* projection of albite–H_2O phase relations.

TABLE 2

Experimental investigations in SiO_2 (quartz)—H_2O and $NaAlSi_3O_8$(albite)—H_2O systems

System	Mineral solubility along the H_2O liquid + vapor coexistence curve	Mineral solubility in supercritical H_2O (V)	Position of the wet solidus and phase compositions	Critical L=V miscibility phenomena	Dry melting curve	Solubility of H_2O in vapor-saturated melt	Position of liquid + gas coexistence curve and critical point of pure dry system
SiO_2-H_2O	Kennedy (1950) Fournier (1960) Kitahara (1960) van Lier and others (1960) Morey and others (1962) Siever (1962) Crerar and Anderson (1971) Mackenzie and Gees (1971) Volosov and others (1972) Hemley and others (1980) Fleming and Crerar (1982) Fournier and Potter (1982) Rimstidt (1997)	Kennedy (1944, 1950) Morey and Hesselgesser (1951) Wasserburg (1958) Wood (1958) Weill and Fyfe (1964) Anderson and Burnham (1965) Sommerfeld (1967) Semenova and Tsiklis (1970) Crerar and Anderson (1971) Nakamura (1974) Fournier and Potter (1982) Ragnarsdóttir and Walther (1983) Walther and Orville (1983) Manning (1994) Manning and Boettcher (1994) Wang and others (2004)	Tuttle and England (1955) Kennedy and others (1962) Stewart (1967) Boettcher (1984) Luth and Boettcher (1986)	Kennedy and others (1962) Stewart (1967) Nakamura (1974)	Jackson (1976) Kanzaki (1990) Hudon and others (2002)	Kennedy and others (1962) Holtz and others (2000)	Guissani and Guillot (1996)
$NaAlSi_3O_8$(albite)-H_2O	*See table notes**	Currie (1968)* Davis (1972)* Woodland and Walther (1987)* Vidale (1983)* Stalder and others (2000)* Shmulovich and others (2001) Hauzenberger and others (2001)* Pak and others (2003)* Shmulovich and others (2006)	Yoder (1958) Bohlen and others (1982) Goldsmith and Jenkins (1985) Luth and Boettcher (1986) Stalder and others (2000)	Boettcher and Wyllie (1969a) Paillat and others (1992) Shen and Keppler (1997)	Schairer and Bowen (1956) Birch and LeComte (1960) Boyd and England (1963) Boettcher and others (1982). Nekvasil and Carroll (1996)	Goranson (1938) Burnham and Jahns (1962) Orlova (1962) Khitarov and others (1963) Luth and others (1964) Kadik and Lebedev (1968) Boettcher and Wyllie (1969a) Morse (1970) Burnham and Davis (1971 & 1974: *PVT* studies) Eggler and Kadik (1979) Voight and others (1981) Day and Fenn (1982) Hamilton and Oxtoby (1986) Richet and others (1986) Paillat and others (1992) Behrens (1995)	*Not determined*

Notes: Studies of amorphous silica, SiO_2 polymorph stabilities and phase relations in the general Na_2O—Al_2O_3—SiO_2±H_2O and related systems are not tabulated. *Solid albite ($NaAlSi_3O_8$) dissolves incongruently/non-stoichiometrically in H_2O.

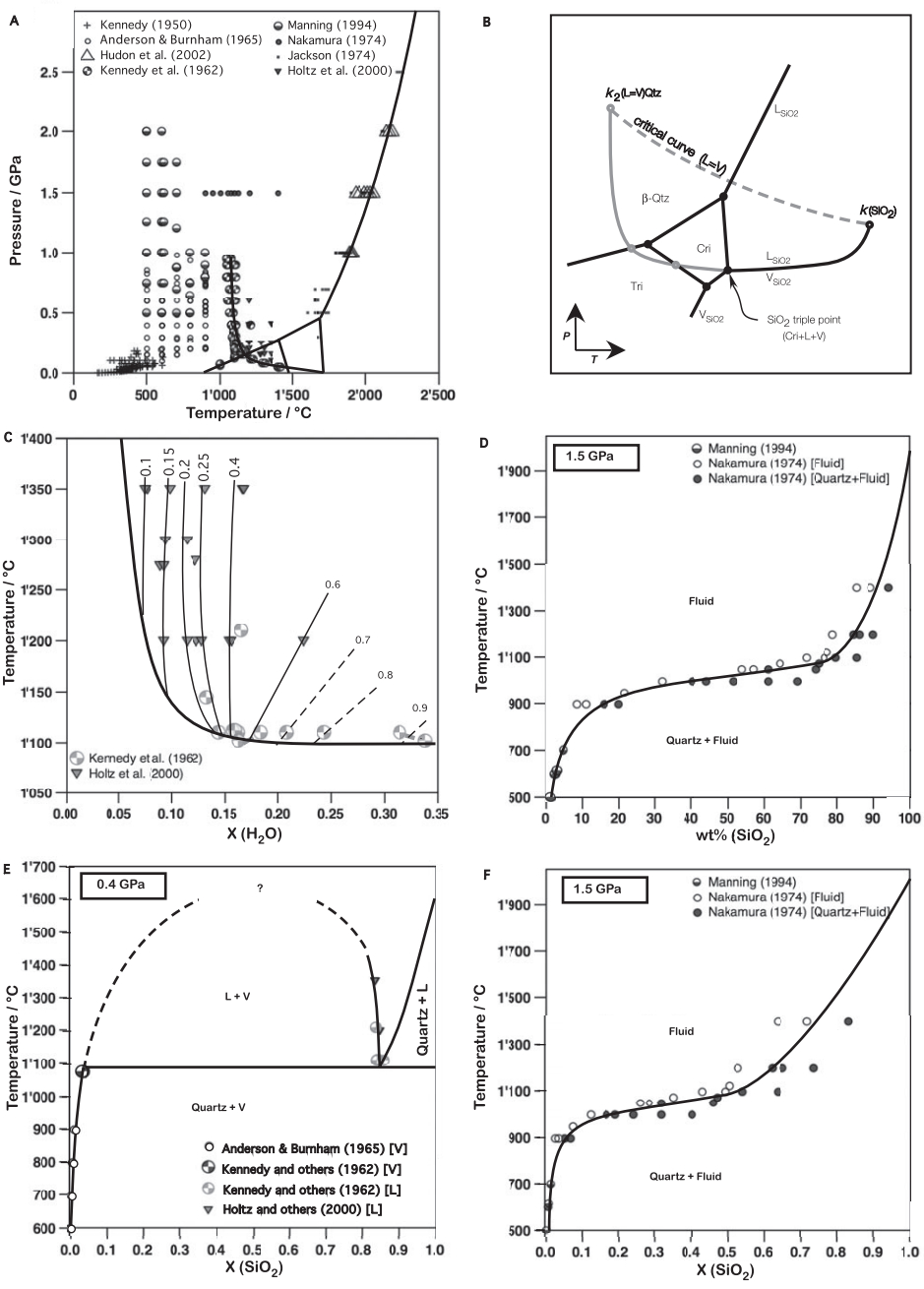

Fig. 5. The SiO_2–H_2O system. (A) Experimental *PT* locations (a selection, table 2). (B) *PT* phase relations near the wet solidus. SiO_2 polymorphs: Tri = tridymite; Cri = cristobalite; β-Qtz = beta-quartz; L = liquid; V = vapor. (C) H_2O solubility (as wt% H_2O) in liquid silica (L) as a function of *T* for various isobars (GPa at ends of steep solid curves). (D) 1.5 GPa quartz solubility/phase equilibria data plotted as weight percent. (E) *TX* section at 0.4 GPa. (F) Figure D replotted as mol fraction $X(SiO_2)$; mw H_2O=18.02, mw SiO_2=60.09.

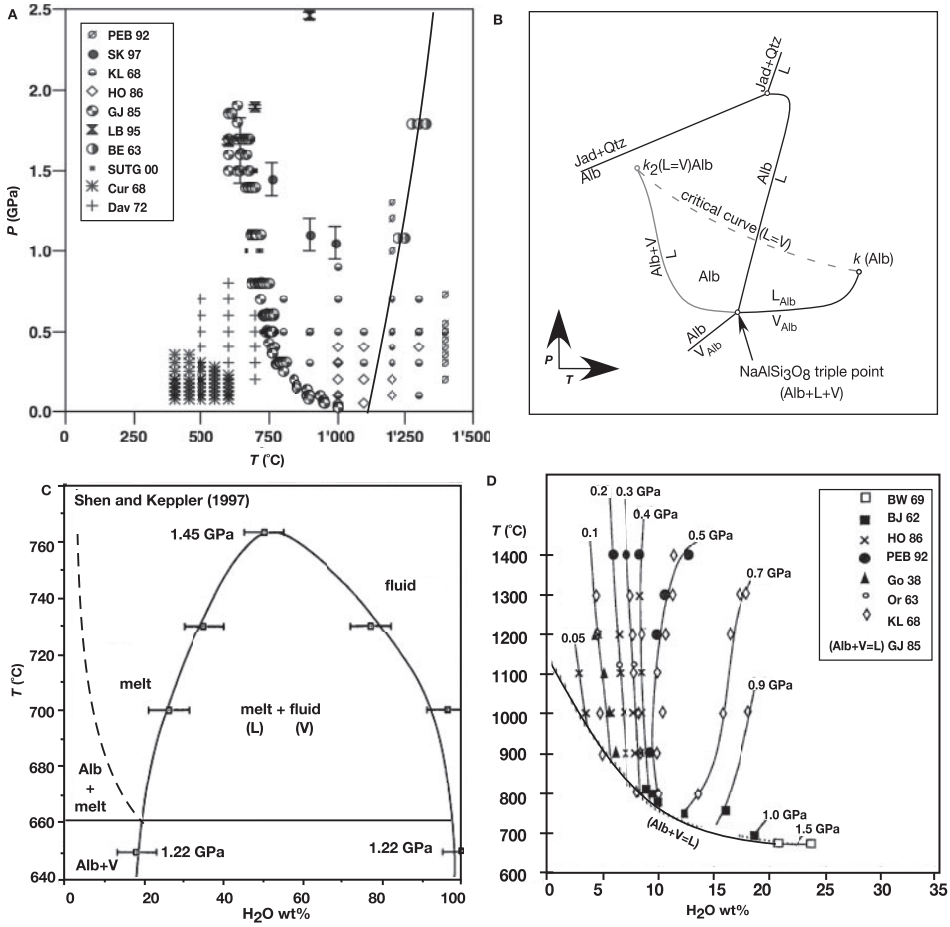

Fig. 6. $NaAlSi_3O_8$(albite)–H_2O phase relations. (A) Experimental data *P*, *T* locations (representative selection, table 1). Dry liquidus (solid line, Alb=L_{Alb}) is shown for reference. (B) Inferred *PT* phase relations for $NaAlSi_3O_8$–H_2O. (C) L+V solvus from Shen and Keppler (1997). Note the data are polybaric, L+V data at 1.22 GPa occur at a *T* below the wet solidius (660 °C) and are metastable. (D) H_2O solubility (as weight percent water) in liquid albite (L) as a function of *T* for various isobars (GPa given at ends of *steep solid curves*) from 0.05 to 1.5 GPa (after Paillat and others, 1992). Data sources, BW: Boettcher and Wyllie (1969b); BJ: Burnham and Jahns (1962); HO: Hamilton and Oxtoby (1986); PEB: Paillat and others (1992, data at 0.35, 0.45 and 0.55 GPa are not plotted in D); Go: Goranson (1938); Or: Orlova (1963); KL: Kadik and Lebedev (1968); GJ 85: Goldsmith and Jenkins (1985); SK 97: Shen and Keppler (1997); LB 95: Liu and Bohlen (1995); BE 63: Boyd and England (1963); SUTG 00: Stalder and others (2000); Cur 68: Currie (1968); Dav 72: Davis (ms, 1972).

Figure 6D shows H_2O solubility in albite-liquid (L) as a function of temperature for a series of pressures (Paillat and others, 1992). Up to 0.4 GPa, H_2O solubility in L decreases with increasing *T* or is neutral, and all data agree well. Above 0.5 GPa, H_2O solubility becomes increasingly prograde with increasing pressure; at 0.7 and 0.9 GPa only the highest values are plotted and these represent a minimum H_2O concentration in L, since exsolution of the dissolved vapor upon quenching made accurate measurements on the glasses difficult (Paillat and others, 1992). The values reported by Paillat and others (1992) at and above 1.0 GPa were inferred by chemographic methods.

Shen and Keppler (1997) located the $NaAlSi_3O_8$–H_2O critical curve (L=V) between 1.0 and 1.5 GPa (fig. 6A) and determined the geometry of the solvus (fig. 6C).

This curve has an overall negative dP/dT slope ($\sim$ -0.55 MPa K^{-1}, assuming linear dP/dT). The intersection of this critical curve with the three-phase curve (Alb+V=L) occurs at 700 °C, 1.6 GPa (Stalder and others, 2000). These observations support the overall topology (type-2, fig. 1B) inferred by Paillat and others (1992).

Several aspects of the $NaAlSi_3O_8$–H_2O system are currently poorly constrained. They include a paucity of information on subsolidus albite solubility in aqueous fluid. Experimentally, albite solubility is complicated by incongruent dissolution. Solubility studies include Currie (1968, reviewed by Fyfe and others, 1978), Anderson and Burnham (1983, a source of data from an unpublished thesis, Davis, ms, 1972), Shmulovich and others (2001), and Antignano and Manning (2003). The composition of vapors coexisting with hydrous albite liquids are also poorly known (although see Clark, 1966, p. 415–436; Boettcher and Wyllie, 1969b).

Although fewer data are available, similar vapor-saturated melt behavior is observed in the system SiO_2–H_2O (fig. 5C). One of the weaknesses in the SiO_2–H_2O data set is limited information on the L+V solvus above the wet solidus. However, a semi-quantitative *PTX* diagram for SiO_2–H_2O can be constructed if it is assumed that L and V isopleths have the same general configuration in this system as in the system $NaAlSi_3O_8$–H_2O.

A Semi-Quantitative Model for the SiO_2–H_2O System

Figure 7 shows the quartz-, melt-, and vapor-saturation isopleth framework for the SiO_2–H_2O system. Figure 7B shows quartz solubility near k_1(L=V)Qtz. Liquid and vapor compositions coexisting with quartz are given by mole fraction H_2O along the isoplethal contours. The experimental data of Kennedy and others (1962) for L and V compositions on the quartz-wet solidus and the quartz solubility data of Anderson and Burnham (1965), Nakamura (1974), and Manning (1994) at 1.5 GPa provide the constraints on the isopleth geometry at P and T above the termination of the wet solidus at k_2(L=V)Qtz. The isopleths for $X(H_2O)^3$ 0.97, at $T < 900$ °C were calculated using the quartz solubility equation of Manning (1994). Elsewhere, the isopleths are fit by hand to the data indicated on figure 5A. The quartz solubility isopleths near the lower S+L+V curve segment (up to 500 °C, 0.1 GPa) are given by mole fraction SiO_2, $X(SiO_2)$, in figure 7B and are fit by hand to the data of Kennedy (1950). No quartz solubility data appear to be available for vapor compositions on the 'lower' S+L+V curve or in the 'gaseous' supercritical region.

The T-dependence of H_2O solubility in vapor-saturated liquid changes as a function of P (fig. 5C). On a contoured PT projection (as in fig. 7), this corresponds to a change in the slope of the respective isopleths from dP/dT near positive or neutral to negative with increasing pressure. This behavior is also present in albite–H_2O (fig. 6D).

SiO_2–H_2O may not be directly relevant to most natural rocks but it does serve to illustrate that topological approaches can be useful for understanding S–L–V phase equilibria that may involve critical behavior.

DISCUSSION

Isopleth dP/dT Slopes, L+V Solvi and Invariant Points

In a pioneering study, Burnham and Davis (1974) used thermodynamic data derived from *PVT* measurements to calculate two divariant equilibria, H_2O solubility in albite liquid at V saturation and the melt composition in equilibrium with albite over a wide range of *PT* conditions, and also the univariant wet solidus equilibrium (Alb+V=L). They predicted that melt isopleths at vapor-saturation would have increasingly positive dP/dT slope with increasing P (see their fig. 18). Such behavior is inconsistent with the L–V solvus found by Shen and Keppler (1997; fig. 6C) and inferred by Paillat and others (1992) which require coexisting L and V isopleths to both have negative dP/dT slope as the L=V curve is approached isobarically with

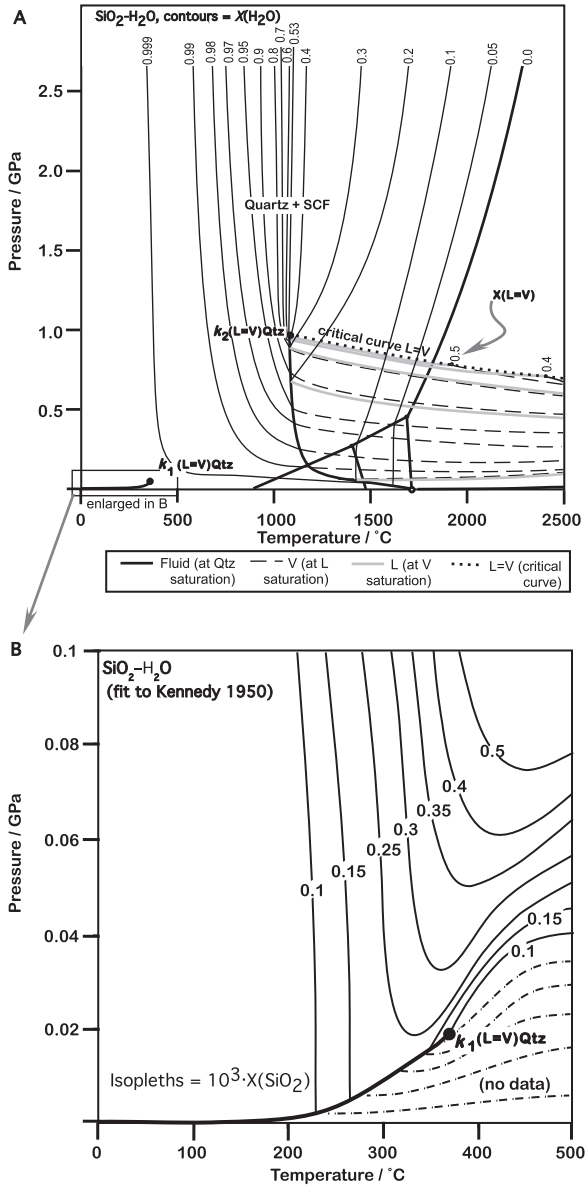

Fig. 7. (A) Semi-quantitative *PTX* projection of solubility and phase relations in the SiO_2–H_2O system consistent with available experimental observations (fig. 5) and assuming the L+V solvus behaves similarly to that observed for $NaAlSi_3O_8$–H_2O. The figure is truncated at 2500 °C for clarity as $k$$SiO_2$ lies at 11,700 °C, ~ 0.2 GPa. The critical isopleth extending from k_2(L=V)Qtz is $X(H_2O)$ = 0.53. The high-temperature part is expected to resemble that shown in fig. 3. (B) Shows quartz solubility isopleths near the lower critical endpoint. At this scale the lower Qtz+V=L curve (due to low solubility) is not distinguished from the L+V coexistence curve for pure H_2O.

increasing *T*. Although their general method was sound, Burnham and Davis (1974) did not correctly predict the L+V solvus behavior with increasing *P*. This highlights the importance of having adequate experimental data to calibrate thermodynamic models, or for our purposes identifying the correct topology.

Geologically, the location of the silicate liquid+vapor coexistence curve and triple point may be of significance for the understanding of condensation of planetary materials from primitive solar nebula (for example, Mysen and Kushiro, 1988). These features are, however, poorly known owing to the extreme conditions where they are likely to occur for refractory geological compounds. If the results of Guissani and Guillot (1996) provide some general guidance, they imply that *k*A occurs at a significantly lower pressure than k_2(L=V)A but also higher pressure than the triple point of pure A. This relative *PT* arrangement differs from previous speculations on the *PT* location of *k*A which place it at higher pressure than k_2(L=V)A (for example, $NaAlSi_3O_8$–H_2O, Wyllie and Tuttle, 1960; SiO_2–H_2O, Tuttle and Bowen, 1958; Krauskopf, 1979), or at equivalent (or lower) pressure than the triple point (for example, $NaAlSi_3O_8$–H_2O, Paillat and others, 1992, see their fig. 7). As noted above, this is significant because the positions of the anhydrous L=V critical point and k_2(L=V)A impose strong constraints on the critical curve, and hence also on the general structure of the fluid+melt solvus, as indicated in figure 4. As an interesting example, it is worth considering the isopleth geometry and critical curve geometry for a system in which H_2O solubility in vapor-saturated liquid increases with increasing *T* at all pressures. This situation implies that the solvus does not change its basic shape as a function of pressure, and hence that there is no d*P*/d*T* reversal in the H_2O solubility curves. Inspection of the topologies discussed indicates that such relations are possible if two distinct regions of L+V immiscibility are present above the wet solidus (fig. 4C).

A Two L+V Solvus A–H_2O Topology

Figure 8 shows the shape of solubility surfaces and phase relations developed where the critical (L=V) curve intersects the anhydrous triple point in a hypothetical system *A*–H_2O. An interesting aspect of this topology is that the high-pressure phase relations are identical to those shown in figure 3, whereas at lower pressure L+V immiscibility can occur in two distinct *PT* regions that are separated by a super-solvus or completely miscible region (fig. 8E). The geometry imposed by the invariant points and the intersecting lines requires that the isopleths for immiscible L+V compositions have a certain d*P*/d*T* slope in each of the separate fields of immiscibility. Thus, vapor- and liquid-isopleths, and the critical curve have negative d*P*/d*T* slopes at temperatures below the triple point, but at higher-temperature, all have positive d*P*/d*T* slopes. Despite the similarities at high pressure, systems like albite–H_2O in which solubility isopleths show an inflection from negative to positive d*P*/d*T* are not part of this topological family because they do not have a temperature interval of complete miscibility between separate L+V solvi (for example, Paillat and others 1992). 'Two-solvi' systems of this type have not yet been described, but the example illustrates how limited solubility data could be used to discriminate between possible topologies and identify the location and geometry of phase equilibrium boundaries.

Critical (L=V) Curve–Wet Solidi Intersections, Non-Intersections and 'Second' Critical Endpoints

The formation of a critical endpoint only occurs where the wet solidus and the L=V critical curve intersect and have the same composition. It is not necessary that all critical (L=V) lines intersect a wet solidus. For example, Boettcher and Wyllie (1969b) noted that wet nepheline melting is strongly incongruent. Hence, L and V compositions on the wet solidus do not lie on the nepheline–H_2O join. This could explain why the nepheline–H_2O critical (L=V) curve (Bureau and Keppler, 1999) crosses the nepheline wet solidus (Boettcher and Wyllie, 1969b) in *PT* without generating a critical endpoint.

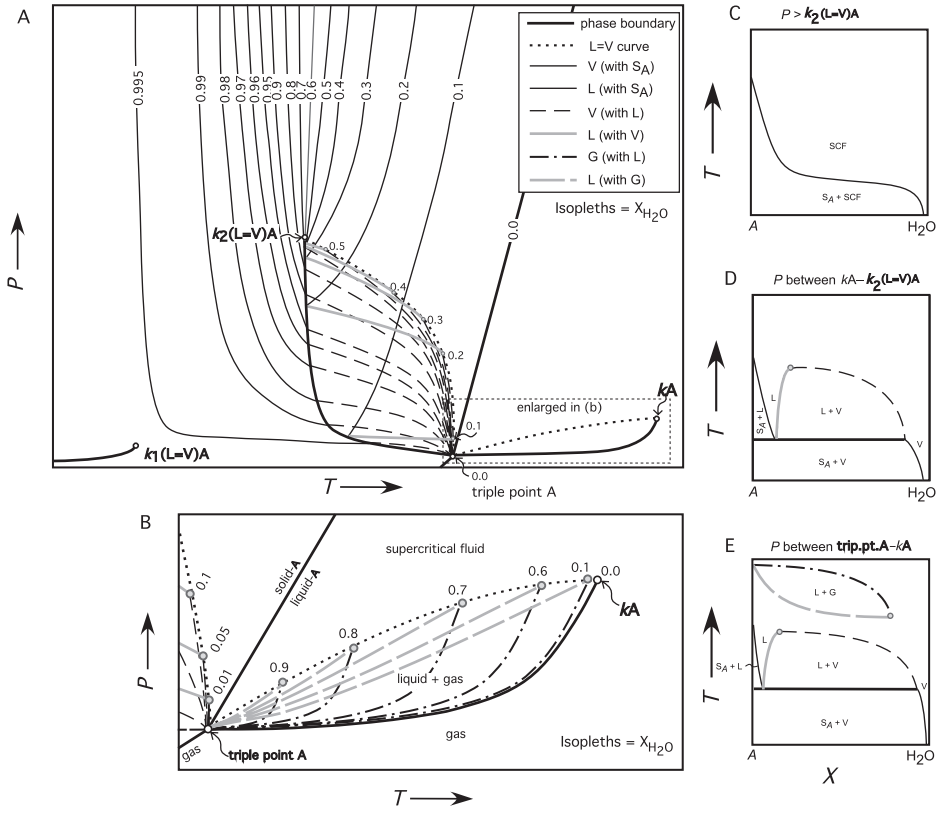

Fig. 8. (A) *PT* projection of binary system *A*–H_2O with two L+V solvi. The two solvi result from the L=V critical curve intersecting the triple point between k_2(L=V) and *k*A from both higher and lower *T*. Isopleth values in $X(H_2O)$. (B) Enlargement of isopleth details for the L+G solvus above dry liquidus. (C–E) show isobaric *TX* sections through the topology.

Is a Critical (L= V) Endpoint on a Wet Solidus Significant?

Recent attention has focused on the occurrence of critical endpoints terminating different wet solidi (for example, Stalder and others, 2000, 2001; Kessel and others, 2005a, 2005b) and the location of L=V critical curves in *PT* space (Shen and Keppler, 1997; Bureau and Keppler, 1999; Sowerby and Keppler, 2002). However, little attention has been given to the structure of the solubility surfaces that give rise to the phase relations being discussed.

Supercritical fluid (melt) compositions can vary continuously with changes in pressure and temperature in the supercritical region, via mineral precipitation and or dissolution. Supercritical phenomena allow fluids to attain hydrous melt-like compositions without passing through a classical melting reaction. Chemically it is not expected that supercritical melts should differ significantly from melts generated via a conventional melting relation at lower pressure on the wet solidus. This is true of the simple *A*–H_2O systems (fig. 3, and SiO_2–H_2O, fig. 7) discussed, and is also supported by recent data on the composition of sub- and supercritical hydrous melts derived from a K-free eclogite (Kessel and others, 2005a, 2005b).

There is a single critical fluid isopleth, extending from the critical endpoint of a wet solidus. If SiO_2–H_2O is any indication, the *PT* trajectory of the critical isopleth

extends smoothly in the direction mimicking a metastable extension of the wet solidus. Supercriticality above a so-called second critical endpoint allows intermediate compositions (between aqueous fluid and silicate melt) to be realized. However, intermediate composition fluids probably only occur in a relatively narrow range of *PT* conditions, which may not be experienced (or only briefly so) in many rocks (Manning, 2004; Hermann and others, 2006).

Fluid Composition, H_2O Activity and Calculated Phase Diagrams

Recognizing regions of low- and high $a(H_2O)$ fluids is important, as calculated phase equilibria at high temperatures and pressures can be very sensitive to this parameter (for example, Powell and others, 2005; Yang and Powell, 2006). Other properties like viscosity and diffusivity are known to be strongly dependent on H_2O content and thus, pressure and temperature are also important. Figures 3, 7 and 8 show how the value of $a(H_2O)$ can vary significantly in *PT* relative to the critical endpoint on a wet solidus when saturated with a solid. It may be justified to assume that $X(H_2O)$ and $a(H_2O)$ are proportional and fixed by the mineral solubility at any given *PT*. In contrast, in fields where two fluid phases are present the relationship between $X(H_2O)$ and $a(H_2O)$ is expected to be complex and non-linear, as is generally the case when a solvus exists.

An important observation from SiO_2–H_2O is that the critical isopleth divides *PT* into a dilute, high-$a(H_2O)$ fluid region and at higher temperature, low-$a(H_2O)$ or solute-rich fluids or supercritical melts occur. The *PT* conditions where intermediate compositions near ~0.5 $X(H_2O)$ occur, fall in a narrow band near the critical isopleth, and hence are comparatively rare in *PT* (Manning, 2004). On the other hand, the band of *PT* where intermediate fluids are stable is likely to vary its position depending on the bulk composition (or mineral+fluid assemblage) of interest, and hence may be more common (or impossible) in certain rocks on specific tectonic *PT* paths.

The relation between *PT* and $a(H_2O)$ is further complicated by other factors that include the presence of soluble salts, like NaCl, that may contribute to enhanced mineral solubility and reduced $a(H_2O)$ at a given *PT* (for example, Aranovich and Newton, 1996, 1997; Newton and Manning, 2002). Thus, although gaps remain, our understanding of fluids and $a(H_2O)$ in high-pressure environments is evolving and should lead to improved calculated fluid-saturated phase diagrams, which may be turned to the task of interpreting natural hydrothermal and wet melting processes.

Geological Applications: Explosive Volcanism, Porphyry Ore Genesis and Subduction Zone Processes

Exsolution of volatiles from magmas is the primary mechanism by which volatile components are liberated from the Earth's interior to the atmosphere and oceans. Volatile saturation determines volcanic eruption styles (Burnham, 1985; Sparks and others, 1994) and is also a fundamental process in the formation of magmatic-hydrothermal ore deposits (Burnham 1979; Hedenquist and Lowenstern, 1994). Understanding *PTX* relations of hydrous magmas provides an insight into processes that drive magmas to exsolve (or resorb) volatile and crystalline components. Similarly, the ability to construct compositionally contoured *PT* surfaces allows fluid-mediated solute transport and melting in metamorphic environments (like dehydration and fluid flow in subduction zone environments), to be conceptually (in the absence of calibrated plots) understood more clearly (Hermann and others, 2006). Analysis of contoured *PT* plots illustrates how subtle differences in solubility surfaces (for example dP/dT slopes and phase relations) between systems are non-trivial as in natural environments they can result in strongly contrasting behavior along different *PT* paths.

CONCLUSIONS

We have constructed a geometrically complete, semi-schematic, general *PTX* model of phase relations and solubility surfaces in silicate–H_2O systems from a critical evaluation of theoretical topological relations and assimilation of published experimental data for the SiO_2–H_2O and $NaAlSi_3O_8$–H_2O systems. The model describes those aspects of basic phase relations for rock–water systems that are poorly known or even unconstrained, and can be used to predict phase stability and the shape of solubility surfaces for fluid phases in *PT* space with limited experimental data. Even if the absolute position of the phase composition isopleths on a *PT* projection is unknown, the isopleth slopes (positive or negative d*P*/d*T*) on the *PT* projection and the compositional range and trends of the isopleths are determined for a given *PTX* topology. The relations between critical fluid compositions and the end of wet melting are made clear.

There is a simple and regular relation between *PT* conditions and the composition of a supercritical fluid where mineral-saturated. In the miscible or supercritical region, a continuum exists between H_2O-rich fluids and supercritical hydrous silicate melt compositions. However, distinct compositional ranges are confined to restricted and well-defined *PT* conditions. Fluid *PTX* domains are correlated with the position and d*P*/d*T* slope of the critical isopleth extending from the critical endpoint on the wet solidus of interest.

The simple approach and examples we describe are conceptually useful for relating solubility surfaces and phase boundary geometries, the design of future experimental studies and understanding large-scale behavior of H_2O-bearing fluid- and melt-interactions with minerals in high *PT* environments.

ACKNOWLEDGMENTS

We thank Maarten Aerts, Jeremy Wykes and Hugh O'Neill for helpful and constructive discussions relating to the work. Reviews by R. Stalder and H. Keppler on an earlier version of the manuscript were appreciated. We thank Craig Manning for providing much helpful and constructive criticism. Thomas Fockenberg and an anonymous reviewer are also thanked for their comments which helped us improve the manuscript.

This work was supported by the Australian Research Council and the Swiss National Science Foundation.

REFERENCES

Ague, J. J., 1994a, Mass-transfer during Barrovian metamorphism of pelites, South-Central Connecticut. 1. Evidence for changes in composition and volume: American Journal of Science, v. 294, p. 989–1057.

——— 1994b, Mass-transfer during Barrovian metamorphism of pelites, South-Central Connecticut. 2. Channelized fluid-flow and the growth of staurolite and kyanite: American Journal of Science, v. 294, p. 1061–1134.

——— 1997, Crustal mass transfer and index mineral growth in Barrow's garnet zone, northeast Scotland: Geology, v. 25, p. 73–76.

Anderson, G. M., and Burnham, C. W., 1965, The solubility of quartz in supercritical water: American Journal of Science, v. 263, p. 494–511.

——— 1983, Feldspar solubility and the transport of aluminum under metamorphic conditions: American Journal of Science, v. 283-A, p. 283–297.

Antignano, A., IV., and Manning, C. E., 2003, Solubility of albite + paragonite ± quartz in H_2O at 1 GPa, 580°C: Implications for metamorphic fluids: American Geophysical Union Fall Meeting, Eos, Transactions, Abstract # V22D-0613.

Aranovich, L. Y., and Newton, R. C., 1996, H_2O activity in concentrated NaCl solutions at high pressures and temperatures measured by the brucite-periclase equilibrium: Contributions to Mineralogy and Petrology, v. 125, p. 200–212.

——— 1997, H_2O activity in concentrated KCl and KCl-NaCl solutions at high temperatures and pressures measured by the brucite-periclase equilibrium: Contributions to Mineralogy and Petrology, v. 127, p. 261–271.

Audétat, A., and Keppler, H., 2004, Viscosity of fluids in subduction zones: Science, v. 303, p. 513–516.

Behrens, H., 1995, Determination of water solubilities in high-viscosity melts: An experimental study on $NaAlSi_3O_8$ and $KAlSi_3O_8$ melts: European Journal of Mineralogy, v. 7, p. 905–920.
Birch, F., and LeComte, P., 1960, Temperature-pressure plan for albite composition: American Journal of Science, v. 258, p. 209–217.
Boettcher, A. L., 1984, The system SiO_2-H_2O-CO_2: melting, solubility mechanisms of carbon, and liquid structure to high pressures: American Mineralogist, v. 69, p. 823–833.
Boettcher, A. L., and Wyllie, P. J., 1969a, The system CaO-SiO_2-CO_2-H_2O III. Second critical end-point on the melting curve: Geochimica et Cosmochimica Acta, v. 33, p. 611–632.
——— 1969b, Phase relationships in the system $NaAlSiO_4$-SiO_2-H_2O to 35 kilobars pressure: American Journal of Science, v. 267, p. 875–909.
Boettcher, A. L., Burnham, C. W., Windom, K. E., and Bohlen, S. R., 1982, Liquids, glasses, and the melting of silicates to high-pressures: Journal of Geology, v. 90, p. 127–138.
Bohlen, S. R., Boettcher, A. L., and Wall, V. J., 1982, The system albite-H_2O-CO_2: a model for melting and activities of water at high-pressures: American Mineralogist, v. 67, p. 451–462.
Boyd, F. R., and England, J. L., 1963, Effect of pressure on melting of diopside, $CaMgSi_2O_6$, and albite, $NaAlSi_3O_8$, in the range up to 50 kilobars: Journal of Geophysical Research, v. 68, p. 311–323.
Bureau, H., and Keppler, H., 1999, Complete miscibility between silicate melts and hydrous fluids in the upper mantle: experimental evidence and geochemical implications: Earth and Planetary Science Letters, v. 165, p. 187–196.
Burnham, C. W., 1979, Magmas and hydrothermal fluids, *in* Barnes, H. L., editor, Geochemistry of hydrothermal ore deposits: New York, John Wiley and Sons, p. 71–136.
——— 1985, Energy-release in subvolcanic environments: Implications for breccia formation: Economic Geology, v. 80, p. 1515–1522.
Burnham, C. W., and Davis, N. F., 1971, Role of H_2O in silicate melts: 1. P-V-T relations in the system $NaAlSi_3O_8$-H_2O to 10 kilobars and 1000 °C: American Journal of Science, v. 270, p. 54–79.
——— 1974, Role of H_2O in silicate melts: 2. Thermodynamic and phase relations in the system $NaAlSi_3O_8$-H_2O to 10 kilobars, 700 ° to 1100 °C: American Journal of Science, v. 274, p. 902–940.
Burnham, C. W., and Jahns, R. H., 1962, A method for determining the solubility of water in silicate melts: American Journal of Science, v. 260, p. 721–745.
Clark, S. P. J., editor, 1966, Handbook of physical constants: Washington, D. C., Geological Society of America Memoir 97, 587 p.
Crerar, D. A., and Anderson, G. M., 1971, Solubility and solvation reactions of quartz in dilute hydrothermal solutions: Chemical Geology, v. 8, p. 107–122.
Currie, K. L., 1968, On solubility of albite in supercritical water in range 400 to 600 °C and 750 to 3500 bars: American Journal of Science, v. 266, p. 321–341.
Davis, N. F., ms, 1972, Experimental studies in the system $NaAlSi_3O_8$-H_2O: the apparent solubility of albite in supercritical water: Pennsylvania State University, Ph. D. thesis, p. 322.
Day, H. W., and Fenn, P. M., 1982, Estimating the P-T-X_{H2O} conditions during crystallization of low-calcium granites: Journal of Geology, v. 90, p. 485–507.
Eggler, D. H., and Kadik, A. A., 1979, The system $NaAlSi_3O_8$-H_2O-CO_2 to 20 kbar pressure. 1. Compositional and thermodynamic relations of liquids and vapors coexisting with albite: American Mineralogist, v. 64, p. 1036–1048.
Ferrando, S., Frezzotti, M. L., Dallai, L., and Compagnoni, R., 2005, Multiphase solid inclusions in UHP rocks (Su-Lu, China): Remnants of supercritical silicate-rich aqueous fluids released during continental subduction: Chemical Geology, v. 223, p. 68–81.
Fleming, B. A., and Crerar, D. A., 1982, Silicic-acid ionization and calculation of silica solubility at elevated-temperature and pH. Application to geothermal fluid processing and reinjection: Geothermics, v. 11, p. 15–29.
Fournier, R. O., 1960, The solubility of quartz in water in the temperature interval from 25 °C to 300 °C: Geological Society of America Bulletin, v. 71, p. 1867–1868.
Fournier, R. O., and Potter, R. W., 1982, An equation correlating the solubility of quartz in water from 25 ° to 900 °C at pressures up to 10,000 bars: Geochimica et Cosmochimica Acta, v. 46, p. 1969–1973.
Fyfe, W. S., Price, N. J., and Thompson, A. B., 1978, Fluids in the Earth's crust: Developments in geochemistry, v. 1: Amsterdam, Elsevier Scientific Publishing Company, 383 p.
Goldsmith, J. R., and Jenkins, D. M., 1985, The hydrothermal melting of low and high albite: American Mineralogist, v. 70, p. 924–933.
Goranson, R. W., 1938, Silicate-water systems: phase equilibria in the $NaAlSi_3O_8$-H_2O and $KAlSi_3O_8$-H_2O systems at high temperatures and pressures: American Journal of Science, Day Volume, v. 35A, p. 71–91.
Guissani, Y., and Guillot, B., 1996, A numerical investigation of the liquid-vapor coexistence curve of silica: Journal of Chemical Physics, v. 104, p. 7633–7644.
Haar, L., Gallagher, J. S., and Kell, G. S., 1984, Steam tables. Thermodynamic and transport properties and computer programs for vapour and liquid states of water in SI units: New York, Hemisphere Publishing, 120 p.
Hamilton, D. L., and Oxtoby, S., 1986, Solubility of water in albite-melt determined by the weight-loss method: Journal of Geology, v. 94, p. 626–630.
Hauzenberger, C. A., Baumgartner, L. P., and Pak, T. M., 2001, Experimental study on the solubility of the "model"-pelite mineral assemblage albite + K-feldspar + andalusite + quartz in supercritical chloride-rich aqueous solutions at 0.2 GPa and 600 °C: Geochimica et Cosmochimica Acta, v. 65, p. 4493–4507.
Hedenquist, J. W., and Lowenstern, J. B., 1994, The role of magmas in the formation of hydrothermal ore deposits: Nature, v. 370, p. 519–527.
Heinrich, C. A., Günther, D., Audétat, A., Ulrich, T., and Frischknecht, R., 1999, Metal fractionation between magmatic brine and vapor, determined by microanalysis of fluid inclusions: Geology, v. 27, p. 755–758.

Hemley, J. J., Montoya, J. W., Marinenko, J. W., and Luce, R. W., 1980, Equilibria in the system Al_2O_3-SiO_2-H_2O and some general implications for alteration-mineralization processes: Economic Geology, v. 75, p. 210–228.

Hermann, J., 2003, Experimental evidence for diamond-facies metamorphism in the Dora-Maira massif: Lithos, v. 70, p. 163–182.

Hermann, J., Spandler, C., Hack, A., and Korsakov, A., 2006, Aqueous fluids and hydrous melts in high-pressure and ultra-high pressure rocks: Implications for element transfer in subduction zones: Lithos, v. 92, p. 399–417.

Holland, T., and Powell, R., 2001, Calculation of phase relations involving haplogranitic melts using an internally consistent thermodynamic dataset: Journal of Petrology, v. 42, p. 673–683.

Holland, T. J. B., 1980, The reaction albite = jadeite + quartz determined experimentally in the range 600-1200 °C: American Mineralogist, v. 65, p. 129–134.

Holland, T. J. B., and Powell, R., 1998, An internally consistent thermodynamic data set for phases of petrological interest: Journal of Metamorphic Geology, v. 16, p. 309–343.

Holtz, F., Roux, J., Behrens, H., and Pichavant, M., 2000, Water solubility in silica and quartzofeldspathic melts: American Mineralogist, v. 85, p. 682–686.

Hudon, P., Jung, I., and Baker, D. R., 2002, Melting of β-quartz up to 2.0 GPa and thermodynamic optimization of the silica liquidus up to 6.0 GPa: Physics of the Earth and Planetary Interiors, v. 130, p. 159–174.

Invernizzi, C., Vityk, M. O., Cello, G., and Bodnar, R. J., 1998, Fluid inclusions in high pressure/low temperature rocks from the Calabrian Arc (southern Italy): the burial and exhumation of the subduction-related Diamante-Terranova unit: Journal of Metamorphic Geology, v. 16, p. 247–258.

Jackson, I., 1976, Melting of silica isotypes SiO_2, BeF_2 and GeO_2 at elevated pressures: Physics of the Earth and Planetary Interiors, v. 13, p. 218–231.

Kadik, A. A., and Lebedev, Y. B., 1968, Temperature dependence of the solubility of water in an albite melt at high pressures: Geochemistry International, v. 5, p. 1172–1181.

Kanzaki, M., 1990, Melting of silica up to 7.0 GPa: Journal of the American Ceramic Society, v. 73, p. 3706–3707.

Kennedy, G. C., 1944, The hydrothermal solubility of SiO_2: Economic Geology, v. 39, p. 25–36.

——— 1950, A portion of the system silica-water: Economic Geology, v. 45, p. 629–653.

Kennedy, G. C., Heard, H. C., Wasserburg, G. J., and Newton, R. C., 1962, The upper three-phase region in the system SiO_2-H_2O: American Journal of Science, v. 260, p. 501–521.

Kessel, R., Schmidt, M. W., Ulmer, P., and Pettke, T., 2005a, Trace element signature of subduction-zone fluids, melts and supercritical liquids at 120-180 km depth: Nature, v. 437, p. 724–727.

Kessel, R., Ulmer, P., Pettke, T., Schmidt, M. W., and Thompson, A. B., 2005b, The water-basalt system at 4 to 6 GPa: Phase relations and second critical endpoint in a K-free eclogite at 700 to 1400 °C: Earth and Planetary Science Letters, v. 237, p. 873–892.

Khitarov, N. I., Kadik, A. A., and Lebedev, Y. B., 1963, Estimate of the thermal effect of the separation of water from felsic melts based on data for the system albite-water: Geokhimiya, v. 7, p. 637–649.

Kitahara, S., 1960, The solubility of quartz in water at high temperatures and pressures: Review of Physical Chemistry of Japan, v. 30, p. 109–114.

Krauskopf, K. B., 1979, Introduction to geochemistry: New York, McGraw-Hill, 617 p.

Levelt Sengers, J. M. H., 2000, Supercritical fluids: Their properties and applications, *in* Kiran, E., Debenedetti, P. G., and Peters, C. J., editors, Supercritical Fluids: NATO Science Series E Applied Sciences, p. 1–30.

Liu, J., and Bohlen, S. R., 1995, Mixing properties and stability of jadeite-acmite pyroxene in the presence of albite and quartz: Contributions to Mineralogy and Petrology, v. 119, p. 433–440.

Luth, R. W., and Boettcher, A. L., 1986, Hydrogen and the melting of silicates: American Mineralogist, v. 71, p. 264–276.

Luth, W. C., Tuttle, O. F., and Jahns, R. H., 1964, The granite system at pressures of 4 to 10 kilobars: Journal of Geophysical Research, v. 69, p. 759–773.

Mackenzie, F. T., and Gees, R., 1971, Quartz: synthesis at Earth surface conditions: Science, v. 173, p. 533–535.

Manning, C. E., 1994, The solubility of quartz in H_2O in the lower crust and upper-mantle: Geochimica et Cosmochimica Acta, v. 58, p. 4831–4839.

——— 2004, The chemistry of subduction-zone fluids: Earth and Planetary Science Letters, v. 223, p. 1–16.

Manning, C. E., and Boettcher, S. L., 1994, Rapid-quench hydrothermal experiments at mantle pressures and temperatures: American Mineralogist, v. 79, p. 1153–1158.

Massonne, H. J., 1992, Evidence for low-temperature ultrapotassic siliceous fluids in subduction zone environments from experiments in the system K_2O-MgO-Al_2O_3-SiO_2-H_2O (KMASH): Lithos, v. 28, p. 421–434.

Morey, G. W., 1957, The solubility of solids in gases: Economic Geology, v. 52, p. 225–251.

Morey, G. W., and Hesselgesser, J. M., 1951, The solubility of quartz and some other substances in superheated steam at high pressures: American Society of Mechanical Engineers, Transactions, v. 73, p. 865–875.

Morey, G. W., and Niggli, P., 1913, The hydrothermal formation of silicates, a review: Journal of the American Chemical Society, v. 35, p. 1086–1130.

Morey, G. W., Fournier, R. O., and Rowe, J. J., 1962, The solubility of quartz in water in the temperature interval from 25° to 300 °C: Geochimica et Cosmochimica Acta, v. 26, p. 1029–1043.

Morse, S. A., 1970, Alkali feldspars with water at 5 kb pressure: Journal of Petrology, v. 11, p. 221–251.

Mysen, B. O., and Kushiro, I., 1988, Condensation, evaporation, melting, and crystallization in the primitive solar nebula: Experimental data in the system MgO-SiO_2-H_2 to 1.0 x 10^{-9} bar and 1870 °C with variable oxygen fugacity: American Mineralogist, v. 73, p. 1–19.

Nakamura, Y., 1974, The system SiO_2-H_2O-H_2 at 15 kbar: Carnegie Institution of Washington Year Book, v. 73, p. 259–263.

Nekvasil, H., and Carroll, W., 1996, Experimental constraints on the compositional evolution of crustal magmas: Journal of the Royal Society of Edinburgh, Earth Sciences, v. 87, p. 139–146.

Newton, R. C., and Manning, C. E., 2002, Experimental determination of calcite solubility in H_2O-NaCl solutions at deep crust/upper mantle pressures and temperatures: Implications for metasomatic processes in shear zones: American Mineralogist, v. 87, p. 1401–1409.

Orlova, G. P., 1962, Solubility of water in albite melts- under pressure: International Geology Reviews, v. 6, p. 254–258.

Paillat, O., Elphick, S. C., and Brown, W. L., 1992, The solubility of water in $NaAlSi_3O_8$ melts: a re-examination of Ab-H_2O phase relationships and critical behaviour at high pressures: Contributions to Mineralogy and Petrology, v. 112, p. 490–500.

Pak, T. M., Hauzenberger, C. A., and Baumgartner, L. P., 2003, Solubility of the assemblage albite + K-feldspar + andalusite + quartz in supercritical aqueous chloride solutions at 650 °C and 2 kbar: Chemical Geology, v. 200, p. 377–393.

Powell, R., Guiraud, M., and White, R. W., 2005, Truth and beauty in metamorphic phase equilibria: Conjugate variables and phase diagrams: Canadian Mineralogist, v. 43, p. 21–33.

Ragnarsdóttir, K. V., and Walther, J. V., 1983, Pressure sensitive silica geothermometer determined from quartz solubility experiments at 250 °C: Geochimica et Cosmochimica Acta, v. 47, p. 941–946.

Ricci, J. E., 1951, The phase rule and heterogeneous equilibrium: New York, D. Van Nostrand Company, Incorporated, 505 p.

Richet, P., Roux, J., and Pineau, F., 1986, Hydrogen isotope fractionation in the system H_2O liquid $NaAlSi_3O_8$: New data and comments on D/H fractionation in hydrothermal experiments: Earth and Planetary Science Letters, v. 78, p. 115–120.

Rimstidt, J. D., 1997, Quartz solubility at low temperatures: Geochimica et Cosmochimica Acta, v. 61, p. 2553–2558.

Rowlinson, J. S., 1983, Critical and Supercritical Fluids: Fluid Phase Equilibria, v. 10, p. 135–139.

Scambelluri, M., and Philippot, P., 2001, Deep fluids in subduction zones: Lithos, v. 55, p. 213–227.

Scambelluri, M., Bottazzi, P., Trommsdorff, V., Vannucci, R., Hermann, J., Gomez-Pugnaire, M. T., and Vizcaino, V. L. S., 2001, Incompatible element-rich fluids released by antigorite breakdown in deeply subducted mantle: Earth and Planetary Science Letters, v. 192, p. 457–470.

Schairer, J. F., and Bowen, N. L., 1956, The system Na_2O-Al_2O_3-SiO_2: American Journal of Science, v. 254, p. 129–195.

Semenova, A. I., and Tsiklis, D. S., 1970, Solubility of silicon dioxide in steam at high pressure and temperatures: Russian Journal of Physical Chemistry, v. 44, p. 1420–1422.

Sharp, Z. D., Essene, E. J., and Hunziker, J. C., 1993, Stable isotope geochemistry and phase equilibria of coesite-bearing whiteschists, Dora-Maira Massif, Western Alps: Contributions to Mineralogy and Petrology, v. 114, p. 1–12.

Shen, A. H., and Keppler, H., 1997, Direct observation of complete miscibility the albite-H_2O system: Nature, v. 385, p. 710–712.

Shmulovich, K., Graham, C., and Yardley, B., 2001, Quartz, albite and diopside solubilities in H_2O-NaCl and H_2O-CO_2 fluids at 0.5-0.9 GPa: Contributions to Mineralogy and Petrology, v. 141, p. 95–108.

Shmulovich, K. I., Yardley, B. W. D., and Graham, C. M., 2006, Solubility of quartz in crustal fluids: experiments and general equations for salt solutions and H_2O-CO_2 mixtures at 400–800 °C and 0.1–0.9 GPa: Geofluids, v. 6, p. 154–167.

Siever, R., 1962, Silica solubility, 0°–200 °C, and the diagenesis of siliceous sediments: Journal of Geology, v. 70, p. 127–150.

Sommerfeld, R. A., 1967, Quartz solution reaction: 400–500 °C, 1000 bars: Journal of Geophysical Research, v. 72, p. 4253–4257.

Sourirajan, S., and Kennedy, G. C., 1962, The system H_2O-NaCl at elevated temperatures and pressures: American Journal of Science, v. 260, p. 115–141.

Sowerby, J. R., and Keppler, H., 2002, The effect of fluorine, boron and excess sodium on the critical curve in the albite-H_2O system: Contributions to Mineralogy and Petrology, v. 143, p. 32–37.

Sparks, R. S. J., Barclay, J., Jaupart, C., Mader, H. M., and Philips, J. C., 1994, Physical aspects of magma degassing I. Experimental and theoretical constraints on vesiculation, *in* Carroll, M. R., and Holloway, J. R., editors, Volatiles in Magmas: Mineralogical Society of America, Reviews in Mineralogy and Geochemistry, v. 30, p. 413–445.

Stalder, R., Ulmer, P., Thompson, A. B., and Günther, D., 2000, Experimental approach to constrain second critical endpoints in fluid/silicate systems: Near-solidus fluids and melts in the system albite-H_2O: American Mineralogist, v. 85, p. 68–77.

——— 2001, High pressure fluids in the system MgO-SiO_2-H_2O under upper mantle conditions: Contributions to Mineralogy and Petrology, v. 140, p. 607–618.

Stewart, D. B., 1967, Four-phase curve in the system $CaAl_2Si_2O_8$-SiO_2-H_2O between 1 and 10 kilobars: Schweizerische Mineralogische und Petrographische Mitteilungen, v. 47, p. 35–59.

Sun, W. D., Bennett, V. C., Eggins, S. M., Kamenetsky, V. S., and Arculus, R. J., 2003, Enhanced mantle-to-crust rhenium transfer in undegassed arc magmas: Nature, v. 422, p. 294–297.

Takenouchi, S., and Kennedy, G. C., 1964, Binary system H_2O-CO_2 at high temperatures + pressures: American Journal of Science, v. 262, p. 1055–1074.

Tödheide, K., and Franck, E. U., 1963, Das Zweiphasengebiet und die kritische Kurve im System Kohlendioxid-Wasser bis zu Drucken von 3500 bar: Zeitschrift für Physikalische Chemie Neue Folge, v. 37, p. 387–401.
Tuttle, O. F., and Bowen, N. L., 1958, The origin of granite in light of experimental studies in the system $NaAlSi_3O_8$-$KAlSi_3O_8$-SiO_2-H_2O: Geological Society of America Bulletin, Memoir, v. 74, p. 153.
Tuttle, O. F., and England, J. L., 1955, Preliminary report on the system SiO_2-H_2O: Geological Society of America Bulletin, v. 66, p. 149–152.
Urusova, M. A., and Valyashko, V. M., 2001, Solubility and immiscibility behavior in ternary hydrothermal systems with critical phenomena in saturated solutions: High Pressure Research, v. 20, p. 447–455.
van Lier, J. A., Debruyn, P. L., and Overbeek, J. T. G., 1960, The solubility of quartz: Journal of Physical Chemistry, v. 64, p. 1675–1682.
Veksler, I. V., 2004, Liquid immiscibility and its role at the magmatic-hydrothermal transition: a summary of experimental studies: Chemical Geology, v. 210, p. 7–31.
Vidale, R., 1983, Pore solution compositions in a pelitic system at high pressures and salinities: American Journal of Science, v. 283A, p. 298–313.
Voight, D. E., Bodnar, R. J., and Blencoe, J. G., 1981, Water solubility in melts of alkali feldspar composition at 5 kb, 950 °C: EOS, v. 62, p. 428.
Volosov, A. G., Khodakov, I. L., and Ryzhenko, B. N., 1972, Equilibrium in system SiO_2-H_2O at elevated temperatures along the lower three-phase curve: Geochemistry International, v. 9, p. 362–377.
Walther, J. V., and Orville, P. M., 1983, The extraction quench technique for determination of the thermodynamic properties of solute complexes: Application to quartz solubility in fluid mixtures: American Mineralogist, v. 68, p. 731–741.
Wang, H. M., Henderson, G. S., and Brenan, J. M., 2004, Measuring quartz solubility by *in situ* weight-loss determination using a hydrothermal diamond cell: Geochimica et Cosmochimica Acta, v. 68, p. 5197–5204.
Wasserburg, G. J., 1958, The solubility of quartz in supercritical water as a function of pressure: Journal of Geology, v. 66, p. 559–578.
Weill, D. F., and Fyfe, W. S., 1964, The solubility of quartz in H_2O in the range 1000-4000 bars and 400-550 °C: Geochimica et Cosmochimica Acta, v. 28, p. 1243–1255.
Wood, J. A., Jr., 1958, The solubility of quartz in water at high temperatures and pressures: American Journal of Science, v. 256, p. 40–47.
Woodland, A. B., and Walther, J. V., 1987, Experimental determination of the solubility of the assemblage paragonite, albite, and quartz in supercritical H_2O: Geochimica et Cosmochimica Acta, v. 51, p. 365–372.
Wyllie, P. J., and Tuttle, O. F., 1960, Experimental investigation of silicate systems containing two volatile components. Part 1: Geometrical considerations: American Journal of Science, v. 258, p. 498–517.
Yang, J. J., and Powell, R., 2006, Calculated phase relations in the system Na_2O-CaO-K_2O-FeO-MgO-Al_2O_3-SiO_2-H_2O with applications to UHP eclogites and whiteschists: Journal of Petrology, v. 47, p. 2047–2071.
Yoder, H. S., Jr., 1958, Effect of water on the melting of silicates: Carnegie Institution of Washington Year Book, v. 57, p. 189–191.